# Nonlinear beamforming for enhancing prestack seismic data with a challenging near surface or overburden

Andrey Bakulin[1], Ilya Silvestrov[1*], Maxim Dmitriev[1], Dmitry Neklyudov[2], Maxim Protasov[2], Kirill Gadylshin[2], Vladimir Tcheverda[2] and Victor Dolgov[3] introduce a new data enhancement algorithm, validate signal-preservation properties and demonstrate applications on challenging land data from an arid environment showing that nonlinear beamforming leads to robust estimation of prestack parameters as well as better imaging.

## Introduction

Modern land seismic data acquisition is moving from sparse grids of large source/receiver arrays to denser grids of smaller arrays or point-source, point-receiver systems. Large arrays were designed to attenuate ground-roll and backscattered noise and to increase overall signal-to-noise ratio (SNR). An example of a typical raw common-shot gather acquired using a legacy acquisition design with 72 geophones in a group and five vibrators per sweep is shown in Figure 1b. We can clearly see that the ground-roll noise with low apparent velocity was partially attenuated by field arrays, and reflection events with high apparent velocity are strong and can be reliably identified. Decreasing the size of field arrays during acquisition in arid environments leads to dramatic decrease in data SNR. An example of raw common-shot gather from a 2D line acquired using a single-sensor survey is shown in Figure 1a. In contrast to legacy data, the single-sensor data is dominated by noise caused by severe multiple scattering in complex near-surface layers and shows no apparent evidence of reflection signal. The sources and receivers were spaced at 10 m intervals in this recent 2D single-sensor survey. This sampling involves much denser acquisition compared to the conventional data using intervals of 30 m or more. Theoretically, high-density seismic acquisition better samples the entire wavefield (signal and noise) and is expected to result in improved imaging. Achieving this in practice with huge amounts of low SNR data proves to be very challenging. Conventional time processing tools such as surface-consistent scaling, deconvolution, static corrections, require reliable prestack signal in the data. Their application to modern seismic datasets acquired with small arrays often leads to unreliable results because the derived operators are based on noise and not on the expected signal. To extract the maximum value from dense high-channel acquisition, we need to enhance signal in the prestack data. Fortunately, densely sampled data gives us more flexibility than grouping geophones directly in the field.

Promising enhancements of very challenging data were obtained recently by supergrouping (Bakulin et al., 2018), that involves local summation of nearby traces. Application of normal moveout (NMO) corrections prior to supergrouping allows handling of larger spatial separation between traces and preserves higher frequencies in the data. An example of supergrouping on 2D single-sensor data after heavy processing and noise attenuation is shown in Figure 4b. The data shows some evidence of coherent reflected events and can be used in later processing. Supergrouping relies on a priori information in the form of global NMO corrections, and in this sense is not data-driven. In the presence of a complex near surface or overburden, the assumption of global hyperbolic NMO may break down and a

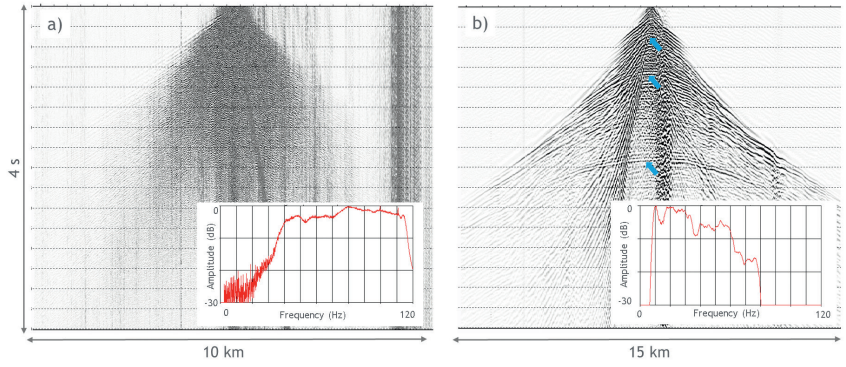


**Figure 1** Comparison of two raw shot gathers including (a) from modern single-sensor acquisition and (b) from legacy acquisition with 72 geophones in a recording group. For single-sensor data the sweep is from 2 Hz to 118 Hz, and for legacy data it is from 4 Hz to 84 Hz. Average amplitude spectrums of the gathers are shown in red. Arrows show reflected events that are observable in the legacy data, while no reflections can be seen in single-sensor data despite significantly increased spatial sampling. Though the gathers are from different areas, they illustrate a typical difference in data quality between two types of acquisition.

[1] Geophysics Technology, EXPEC Advanced Research Center, Saudi Aramco
[2] Institute of Petroleum Geology and Geophysics, Novosibirsk, Russia | [3] Geophysical Data Processing Division, Saudi Aramco
[*] Corresponding author, E-mail: ilya.silvestrov@aramco.com

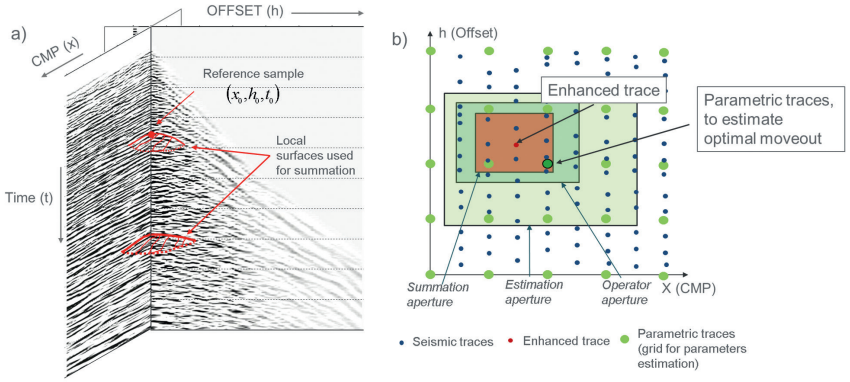


**Figure 2** Schematics of the data enhancement process showing (a) input data in the common midpoint-offset domain where the data samples are stacked along the local traveltime surfaces and (b) data apertures for estimating the kinematic operators by means of automatic coherency analysis. If a parametric trace is within an operator aperture from the reference enhanced trace then the local traveltime surface is constructed corresponding to this parametric trace. All samples located on this surface within the summation aperture around the reference trace are stacked together to form the output sample. As a rule, several parametric traces usually fall inside the operator aperture, and therefore aggregate output consists of several combinations summed along multiple trajectories.

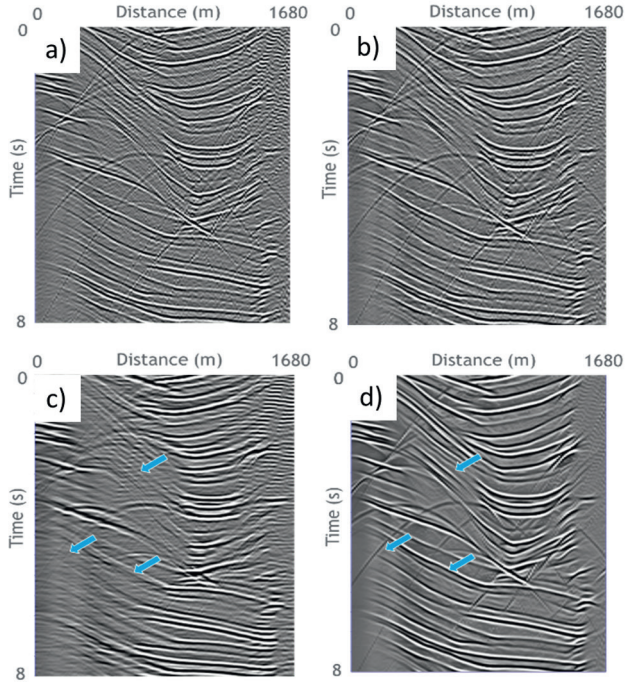


**Figure 3** Synthetic data example showing a common-offset gather (a) after supergrouping (80-m aperture), (b) after nonlinear beamforming (80-m aperture), (c) after supergrouping (300-m aperture), and (d) nonlinear beamforming (300-m aperture). Arrows mark areas showing significant attenuation for diffractions and steeper events after supergrouping using a larger aperture. Nonlinear beamforming continues to preserve most of these events including those with conflicting dips.

more sophisticated approach is desired that can estimate actual moveout directly from the data.

Multi-dimensional data-driven stacking techniques, such as the common-reflection surface method (CRS) or multi-focusing (MF), have been widely used in the past to get better stack sections and to enhance prestack gathers (Mann et al., 1999; Al-Marzoug et al., 2008; Baykulov and Gajewski, 2009; Curia et al., 2017). These methods assume a global trajectory of the reflection events, which may fail in complex geological conditions. Non-zero offset CRS and non-hyperbolic MF methods were proposed to avoid global hyperbolic approximations and to use local kinematic wavefield parameters (Zhang et al., 2001; Muller and Spinner 2010; Berkovitch et al., 2011). A similar approach was presented by Buzlukov et al. (2010) and Buzlukov and Landa (2013) who proposed enhancing prestack data in the common-offset domain based on searching for locally coherent events in the data and then partial summing along the estimated trajectories. Unlike CRS or MF techniques, they used localized second-order approximation of travel-time surfaces without assigning specific meaning to model-based parameters. Such multi-dimensional data stacking can be considered as a delay-and-sum beamforming method. Unlike conventional beamforming (slant stack), the time delay in this approach is a nonlinear function of distance. In the current work we introduce such nonlinear beamforming in the CMP-offset domain for enhancing challenging prestack land seismic data with low signal-to-noise ratio caused by strong near-surface scattering. Nonlinear beamforming is a flexible tool and can be used to enhance different types of events including primary reflections, refractions, head waves, converted waves and diffractions.

## Method

Each trace in a seismic volume can be defined by midpoint and offset co-ordinates. For trace enhancement, nonlinear beamforming comprises a local summation of nearby traces after application of time shifts. Formally it can be written as local summation over a traveltime surface of the form:

$$u(x_0, h_0, t_0) = \sum_{(x,h)\in B_0} w(x, h)u(x, h, t_0 + \Delta t(x,h)), \quad (1)$$

where $u(x,h,t)$ represents a trace with midpoint and offset co-ordinates, $x$ and $h$, respectively. The co-ordinates of the output trace after the beamforming procedure are given by $x_0$, $h_0$. The summation is done over a local region $B_0$ around the output trace in CMP-offset plane along a traveltime surface with some moveout $\Delta t(x,h)$. The main assumption is that the wavefront can be locally approximated by a second-order surface as follows:

$$\Delta t(x,h) = t(x,h) - t_0(x_0,h_0) = A\Delta x + B\Delta h + C\Delta x\Delta h + D\Delta x^2 + E\Delta h^2,$$

where $\Delta x$, $\Delta h$ represent distances along midpoint and offset axis with respect to the output trace (Figure 2) and $A,B,C,D,E$ are unknown local kinematic parameters (first and second order traveltime derivatives) that should be estimated.

The beamforming weights $w(x,h)$ can be chosen in a number of ways to enhance signal energy and to suppress noise. Various sophisticated approaches can be adopted in this scheme to preserve intra-array static time shifts and other local peculiarities of the wavefield. The estimated kinematic parameters have

particular physical meaning in models of mild complexity. For example, the A and D parameters correspond to slope and curvature of events in common-offset sections and are related to structural characteristics of the model. The B and E parameters define slope and curvature of events in the common-midpoint domain and are related mostly to the model velocity. The mixed parameter C connects the two domains. These parameters are related to a common-offset CRS operator (Zhang et al., 2001) and to a non-hyperbolic multi-focusing operator (Berkovitch et al., 2011) and in simplified cases can be derived through them. The optimal values of $A,B,C,D,E$ are obtained by means of coherence analysis similar to CRS or multi-focusing techniques during the estimation stage.

During the estimation stage, we follow a similar approach to Hoecht et al. (2009) and first make a two-parameter scan for A and D, followed by a scan for B and E. Finally, we fix the four estimated coefficients and search for an optimal value of C. To avoid unwanted events and to improve search efficiency, we apply normal-moveout (NMO) correction prior to data enhancement. This enables the use of stacking velocities as a guide during the parameter estimation process and the user defines how far the scanning parameters can deviate from this guide. To improve the results and efficiency of the search, an operator-oriented approach was implemented (Hoecht et al., 2009). In this approach, the moveout coefficients are estimated on a coarse grid in the CMP-offset plane using all traces falling inside an estimation aperture (Figure 2b).

After the estimation step, traveltime operators are constructed around all parametric traces. For each actual trace, the traces falling inside the summation aperture are summed according to equation (1). The summation operators are taken from the parametric traces falling inside the operator aperture around the actual trace. This approach allows us to bring signal in each sample from different estimated operators giving high fold and also partially reconstructing events with conflicting dips. The computational cost of such operator-oriented stacking is significantly higher than simple grouping of traces in supergrouping. To speed up this stack, a special 'parametric trace-oriented' summation algorithm was developed, in which the signal is first accumulated in the parametric traces and only then is moved to the target output traces. Compared to the conventional approach that accumulates signal in the target traces from the very beginning, this gives a significant speed up in the summation phase.

## Synthetic data example

To demonstrate the benefits of nonlinear beamforming in comparison to simpler approaches, such as supergrouping, we use a synthetic example from the Sigsbee model similar to the CRS example presented in Baykulov and Gajewski (2009). The main goal is to validate the ability of the method to preserve signal and therefore a noise-free synthetic dataset is used. In Figure 3a we show a common-offset gather after supergrouping of traces with a summation aperture of 80 m in both mid-point and offset directions. The result is almost identical to the original common-offset gather (not shown here). The nonlinear beamforming algorithm results in the gather shown in Figure 3b. Coherent events are preserved while some slight incoherent features of the wavefield are treated as noise and are suppressed. Local summation with a much larger aperture of 300 m reveals big differences between the two approaches. As expected, supergrouping of traces suppresses steeply dipping events including strong diffractions with hyperbolic shapes (Figure 3c). In contrast, nonlinear beamforming preserves most of the events despite a large summation aperture (Figure 3d). An operator-oriented approach with partial summation is also able to preserve most of the conflicting dips in this example.

## Real data examples

### *Imaging and velocity analysis using point-source point-receiver data*

In the first real-data example, we apply nonlinear beamforming to the point-source, point-receiver 2D dataset shown in Figure 1a. After conventional noise attenuation, a common-shot gather still reveals an extreme degree of near-surface scattering, which completely obscures the reflections (Figure 4a). After applying NMO and supergrouping in the receiver domain with a 140-m aperture (Bakulin et al., 2018) we start to observe some hints of reflections (Figure 4b) albeit very weak. Note that simply filtering this result (Figure 4b) does not improve events coherency. Nonlinear beamforming with a summation aperture

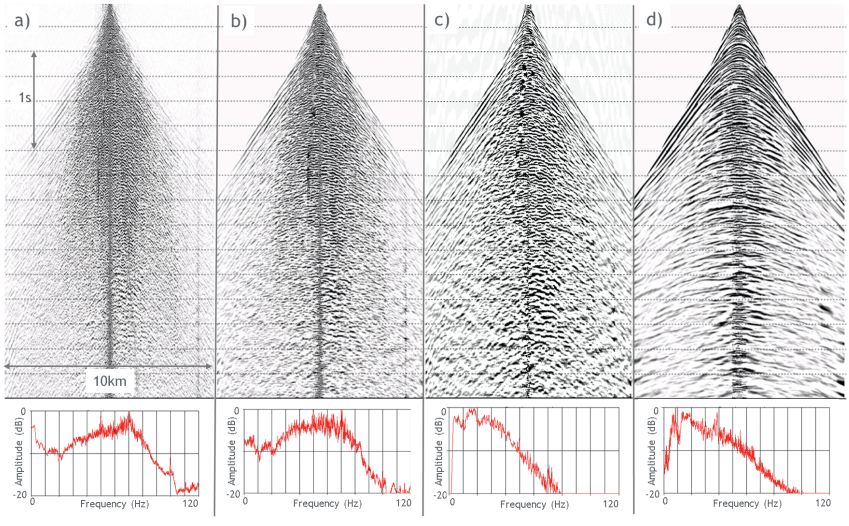


**Figure 4** Single-sensor data from Figure 1a after heavy noise attenuation using (a) conventional processing, (b) conventional processing and supergrouping, (c) conventional processing and supergrouping and band-pass filtering, and (d) conventional processing and supergrouping and nonlinear beamforming. Average amplitude spectrums of the gathers are shown in red.

diameter of 300 m results in much stronger, more coherent reflections (Figure 4d). Figure 5 shows that a time-migrated image of data after nonlinear beamforming provides superior image quality compared to an image of supergrouped traces. We observe a clear improvement in reflector continuity and strength especially in challenging zones. The image after nonlinear beamforming shows some deficiency in higher frequencies. This is most probably owing to filtering of high-frequency noise and not suppression of the signal. Note that these images were constructed using identical velocities. It is expected that the improvement in SNR of the prestack gathers should improve the velocity analysis, surface-consistent processing, statics estimation and deliver even better final results (Bakulin and Erickson, 2017). Figure 6 shows how velocity semblance panels are improved after nonlinear beamforming compared to using the original data and to supergrouping results. The initial velocity that was used as a guide in beamforming is shown as a black line. In this example, the velocity of events during the automatic coherency scan are perturbed up to 10%. Even though this was done locally for each point in the CMP-offset section lying on a 150x100 m grid, we observe a clear improvement in the quality of the semblance maxima now clustering around the guide velocity. This suggests that better velocities can be estimated using enhanced data. Nonlinear beamforming employs massive partial stacking from neighbouring midpoint positions and reveals reflection events not visible in the original data.

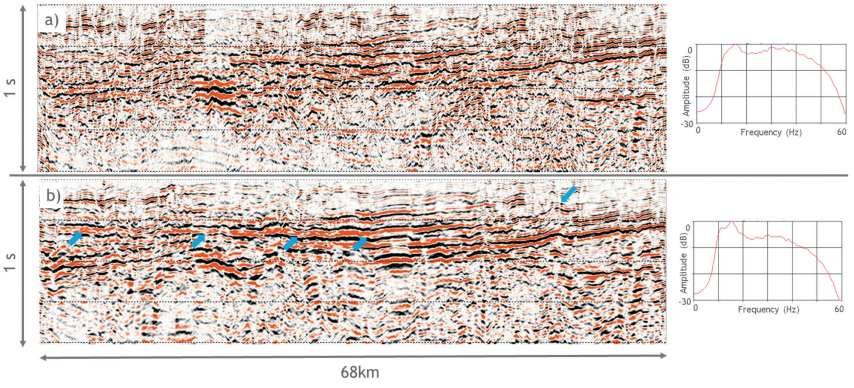


**Figure 5** Time-migrated images of 2D point-source, point-receiver data obtained with (a) supergrouping in the common-shot domain with 140-m aperture, and (b) nonlinear beamforming with a 300-m aperture. Average amplitude spectrums of the images are shown in red.

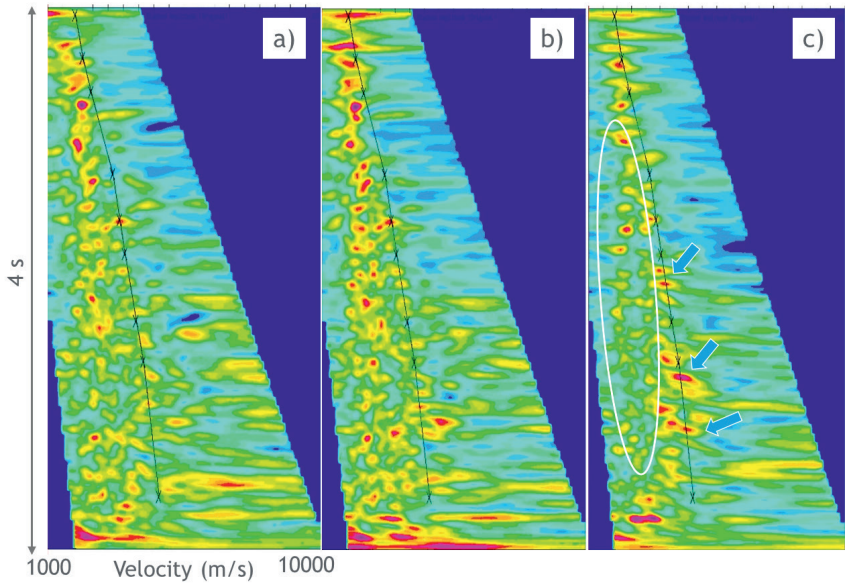


**Figure 6** Semblance panels obtained during conventional P-wave velocity analysis using (a) original data, (b) data after supergrouping, and (c) data after nonlinear beamforming. The black line shows the guide velocity function used during beamforming. The white ellipse indicates a zone with suspected multiples prominent on (a) and (b) and greatly reduced on (c).

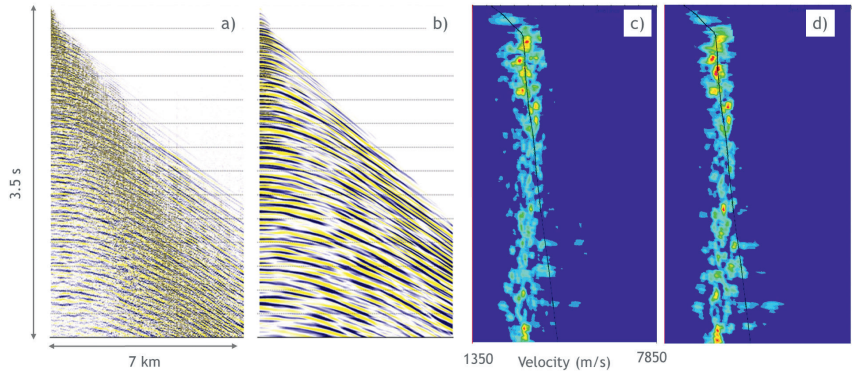


**Figure 7** Application of nonlinear beamforming to legacy 2D data acquired with 72-geophone receiver groups and five vibrators in each source array. A CMP from a good-quality area is shown (a) before NLBF, (b) after NLBF, along with the velocity semblance panels, (c) before NLBF and (d) after NLBF. Note that additional processing was applied to the gathers shown in (a) and (b) before calculating the semblance. Observe that NLBF sharpens semblance panels, but generally gives the same velocity trend.

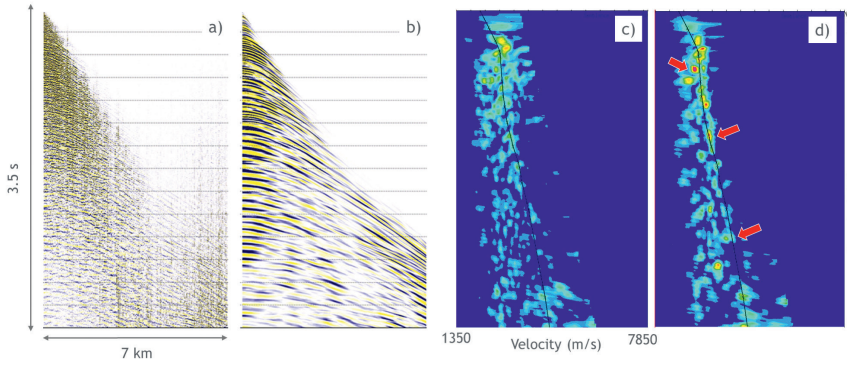


**Figure 8** Application of nonlinear beamforming to the same legacy 2D line as in Figure 7, but now in a challenging area. A CMP gather is shown (a) before NLBF, (b) after NLBF and the corresponding coherency panels, (c) before NLBF, and (d) after NLBF. Note that additional processing was applied to the gathers shown in (a) and (b) before calculating the semblance. Observe that panels after NLBF reveal more maxima in the vicinity of the black guide function and enable more reliable velocity picking.

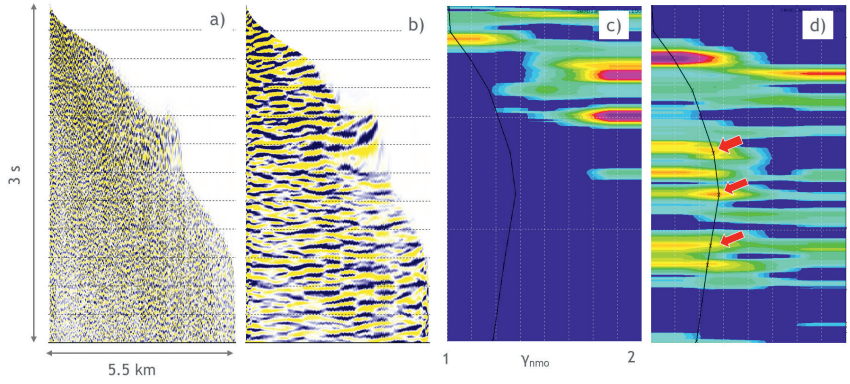


**Figure 9** An example of NLBF for converted wave velocity analysis of 3D 3C land data using a common-conversion point (CCP) gather from single-sensor data showing the radial component of the wavefield (a) before NLBF, (b) after NLBF, along with the corresponding coherency panels used for $\gamma_{nmo}$ picking (c) before NLBF, and (d) after NLBF. Nonlinear beamforming reveals much more coherent events on enhanced gathers and produces meaningful semblance maxima on coherence panels.

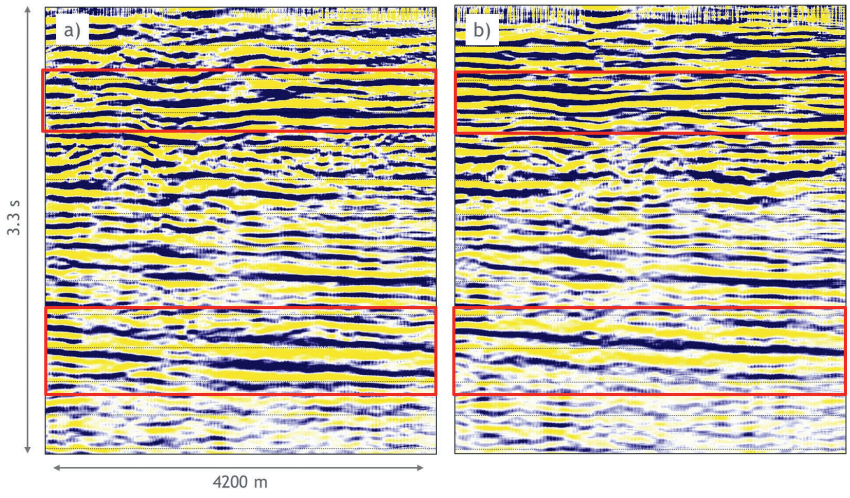


**Figure 10** Converted-wave (PS) stacked sections obtained from single-sensor data using $\gamma_{nmo}$ values picked on (a) original data, and (b) on data after NLBF enhancement. Note the input data to the stack is the same in both panels.

We also note that the beamforming also partially suppresses multiples as confirmed by reduced energy inside the white ellipse in Figure 6c.

### *Velocity analysis of data with large field arrays*

The second example comprises a conventional land seismic dataset from an area with strongly variable near-surface conditions. This 2D data was acquired with 30 m sampling for both sources and receivers, and using 72-geophone receiver arrays and source arrays with five vibrators. A common-midpoint gather after preprocessing and noise attenuation from a relatively good quality area is shown in Figure 7a. In this case, field arrays did quite a good job attenuating surface wave and backscatter noise and we can observe some coherent events in the prestack data. After nonlinear beamforming, the events became much more visible and continuous from top to bottom. The enhanced gathers do not reveal new information in terms of velocity as can be seen from comparison of NMO semblance panels obtained before and after NLBF (Figure 7c,d). Some events became more coherent but overall the semblance maxima before and after beamforming maintain similar positions. In contrast, application of NLBF to a relatively bad-quality area from the same line provides more focused semblance panels and improved stacking velocity picks as can be seen in Figure 8. Despite using large arrays in the field, the data in this area show little evidence of reflections, as can be seen from velocity panels, which show weak and scattered semblance peaks covering the whole time interval. In contrast, the corresponding gather after enhancement (Figure 8b) clearly reveals reflection events. The semblance panels reveal robust maxima located in the vicinity of the guide velocity function. Coherency panels after enhancement reach acceptable quality for reliable velocity analysis.

### *Converted-wave velocity analysis using 3D 3C point-receiver data*

In the next example we apply NLBF to improve results of multi-component processing of single-sensor 3D 3C data. In this processing P- and S-wave velocity ratios ($\gamma_{nmo}$) need to be picked to estimate an converted-wave stacking velocity model. After rotating the recorded 3C data, we obtain the radial component of the wavefield (Figure 9) sorted as a common-conversion-point (CCP) gather. The data are extremely noisy and contain no visible coherent events suitable for reliable $\gamma_{nmo}$ picking. To enhance the PS mode conversions, common-conversion-point moveout corrections are applied based on PP reflections and some initial fixed $\gamma_{nmo}$ value. NLBF is then used to explore coherency within wide ranges of dips and curvatures, which enables it to find and enhance converted-wave events on the radial component. CCP gathers are then obtained with significantly improved signal-to-noise ratio that enables reliable picking of the $\gamma_{nmo}$ values. The stacked sections obtained using picks based on the original data and the new data after enhancement are compared in Figure 10. There is a significant improvement in event continuity across the entire section in Figure 10b, suggesting that converted-wave velocity obtained after NLBF makes better geological sense.

## Conclusions

Nonlinear beamforming is applied to challenging land seismic data corrupted by strong scattering noise caused by a complex near surface. The approach estimates local nonlinear coherent events in the data and performs partial summation along them. This method does not rely on classical hyperbolic assumptions described by global moveout across an entire range of offsets. Instead, it utilizes a local second-order approximation of travel-times with kinematic parameters evaluated directly from the data and varying spatially and with time/depth. Preliminary stacking velocities can be used as a guide, therefore allowing the method to suppress unwanted events such as backscattered noise and multiples and enhanced reflection events. The enhanced data provides significant benefits for many stages of the processing flow. We presented land data examples from a desert environment with a complex near surface, focusing on velocity estimation and imaging. We expect that nonlinear beamforming might lead to a breakthrough in processing of modern high-channel count and signal-sensor data and should enable the extracting of the maximum usable information, especially in the presence of a complex overburden.

## Acknowledgments

We would like to thank Evgeny Landa for inspiring discussions and Mohammed Mubarak for useful suggestions and for help with the real data example.

## References

Al-Marzoug, A.M., Ahmed, F.Y. and Sliz, K.K. [2008]. Seismic imaging and velocity model building using common reflection surface stack. *First Break,* **26**(2), 99-104.

Bakulin, A., Golikov, P., Dmitriev, M., Neklyudov, D., Leger, P. and Dolgov, V. [2018]. Application of supergrouping to enhance 3D prestack seismic data from a desert environment. *The Leading Edge*, **37**(3), 200–207.

Bakulin, A. and Erickson, K. [2017]. Enhance—estimate—image: New processing approach for single-sensor and other seismic data with low prestack signal-to-noise ratio. *87th Annual International Meeting, SEG*, Expanded Abstracts, 5001-5005

Baykulov, M. and Gajewski, D. [2009]. Prestack seismic data enhancement with partial common-reflection-surface (CRS) stack. *Geophysics*, **74**, V49-V58.

Berkovitch, A., Deev, K. and Landa E. [2011]. How non-hyperbolic Multi-Focusing improves depth imaging. *First Break*, **29**, 103-111.

Buzlukov, V., Baina, R. and Landa, E. [2010]. Prestack data enhancement using local traveltime approximation. *72nd EAGE Conference and Exhibition*, Expanded Abstract, C011.

Buzlukov, V. and Landa, E. [2013]. Imaging improvement by prestack signal enhancement. *Geophysical Prospecting*, **61**, 1150-1158.

Curia, D., Borghi, P., Noble, J., Berkovitch, A., Justo, D. and Alayón, M. [2017]. The impact of multifocusing in the processing of land 3D seismic data in a fold and thrust belt setting: Ranquil Norte Block, Neuquén Basin, Argentina. *The Leading Edge*, **36**(9), 770–774.

Hoecht, G., Ricarte, P., Bergler, S. and Landa, E. [2009]. Operator-oriented interpolation. *Geophysical Prospecting* **57**, 957-981.

Mann, J., Jagar, R., Muller, T., Hocht, G. and Hubral, P. [1999]. Common-reflection-surface stack – a real example. *Journal of Applied Geophysics*, **42**(3), 301-318.

Mueller, N., A., Spinner, M. [2010]. Improving Prestack Migration with CRS Techniques–A Case Study, *72nd EAGE Conference and Exhibition*, Expanded Abstract, D032.

Zhang, Y., Bergler, S. and Hubral, P. [2001]. Common-reflection-surface (CRS) stack for common offset. *Geophysical Prospecting*, **49**, 709-718.